FEATURE ARTICLE

Hydrophobic Effects on a Molecular Scale

G. Hummer,* S. Garde, A. E. García, M. E. Paulaitis,[†] and L. R. Pratt

Theoretical Division, Los Alamos National Laboratory, Los Alamos, New Mexico 87545, and Department of Chemical Engineering, Johns Hopkins University, Baltimore, Maryland 21218

Received: July 2, 1998; In Final Form: September 25, 1998

A theoretical approach is developed to quantify hydrophobic hydration and interactions on a molecular scale, with the goal of insight into the molecular origins of hydrophobic effects. The model is based on the fundamental relation between the probability for cavity formation in bulk water resulting from molecular-scale density fluctuations and the hydration free energy of the simplest hydrophobic solutes, hard particles. This probability is estimated using an information theory (IT) approach, incorporating experimentally available properties of bulk water: the density and radial distribution function. The IT approach reproduces the simplest hydrophobic effects: hydration of spherical nonpolar solutes, the potential of mean force (PMF) between methane molecules, and solvent contributions to the torsional equilibrium of butane. Applications of this approach to study temperature and pressure effects provide new insights into the thermodynamics and kinetics of protein folding. The IT model relates the hydrophobic-entropy convergence observed in protein unfolding experiments to the macroscopic isothermal compressibility of water. A novel explanation for pressure denaturation of proteins follows from an analysis of the pressure stability of hydrophobic aggregates, suggesting that water penetrates the hydrophobic core of proteins at high pressures. This resolves a long-standing puzzle, whether pressure denaturation contradicts the hydrophobic-core model of protein stability. Finally, issues of "dewetting" of molecularly large nonpolar solutes are discussed in the context of a recently developed perturbation theory approach.

I. Introduction

Hydrophobic interactions play a central role in many self-assembly processes in aqueous solution: protein folding; the formation of micelles, membranes, and complex mesophases in surfactant solutions; the formation of macromolecular complexes; and the nonspecific aggregation of proteins in inclusion bodies during overexpression or in disease-causing amyloid plaque formation in brain tissue.[1-5] Biopolymers such as proteins, nucleic acids, and lipids contain a significant fraction of nonpolar groups: aliphatic and aromatic amino-acid side chains, the faces of nucleic-acid bases, and the hydrocarbon tails of lipids. Attractive hydrophobic interactions between these nonpolar groups contribute significantly to the stability of folded proteins, base-stacking in helical nucleic acids, and membrane bilayers. Protein folding may be the most extensively characterized macromolecular self-assembly process in aqueous solution. Thermodynamic[1,2,6-8] and structural studies[9,10] on proteins have shown that the formation of a hydrophobic core, comprising predominantly nonpolar amino acids, plays a significant if not the dominating role in protein folding. Clearly, other interactions, such as electrostatic interactions and intramolecular or water-mediated hydrogen bonding, cannot be neglected in a complete treatment of the thermodynamic stability of amphiphilic molecules and their assemblies. Nevertheless, a quantitative understanding of the stability of hydrated am-

* Corresponding Author. Mail Stop K710. Phone: (505) 665-1923. Fax: (505) 665-3493. E-mail: hummer@lanl.gov.
[†] Department of Chemical Engineering.

phiphilic macromolecules necessitates a thorough, quantitative description of hydrophobic driving forces as a major contributing factor.

Despite many decades of research on hydrophobic effects, our understanding of key phenomena presumably of hydrophobic origin is still incomplete, and seemingly contradictory observations have yet to be explained. Surprisingly, these include the effects of changing even the most elementary thermodynamic variables, temperature and pressure, or key solution properties, such as salt concentration and composition. The well-known fact that proteins denature at elevated temperatures and at elevated pressures is an immediate example. Heat denaturation can be explained by the hydrophobic core model of proteins, which was established on the basis of extensive temperature unfolding studies.[6−8,11,12] These studies show that the thermodynamic characteristics of heat denaturation are similar to those of transferring nonpolar molecules from a hydrocarbon or gas phase into water. This suggests that nonpolar residues in the protein interior become exposed to solvent during denaturation. However, as pointed out poignantly by Kauzmann,[13] pressure denaturation appears to contradict the hydrophobic-core model of proteins in the sense that the hydrocarbon transfer process and protein denaturation exhibit diametrically opposite pressure dependences of the associated volume change.

One goal of our work has been to reconcile these apparently contradictory results for temperature and pressure denaturation of proteins within the context of the hydrophobic core model of protein folding. To achieve this, we developed detailed molecular explanations for the underlying processes.[14,15] Here, we will focus specifically on the observed temperature convergence of hydrocarbon-transfer entropies from calorimetry experiments.[14] That entropy convergence coincides with the observed temperature convergence of the entropy of protein unfolding and thus provides a thermodynamic foundation for the hydrophobic-core model of protein folding.[6,7,11,12,16−18] In addition, we will suggest a molecular mechanism for pressure denaturation of proteins[19−26] and discuss its consequences on folding kinetics and the characteristics of the ensemble of unfolded protein structures.[15] Our explanation of pressure denaturation invokes experimental observations regarding the differences in the structures of heat and pressure-denatured proteins, the latter being more compact.[23,27,28] We will also give preliminary results for the effects of salt concentration on hydrophobic hydration, as characterized by the Hofmeister series,[29] which ranks salts by their ability to increase ("salt in") or decrease ("salt out") the solubility of nonpolar molecules in water.

To achieve these goals, we need a model that quantifies hydrophobic hydration and hydrophobic interactions, and the effects of temperature, pressure, and salt concentration on them. A number of models of the hydrophobic effect have been developed in the past,[1,2,4,30−34] all having their merits and limitations.[35] One of the most influential models is scaled-particle theory (SPT)[36] and its extension to hydrophobic hydration.[37,38] SPT laid a molecular foundation for surface area models of hydrophobic hydration with macroscopic surface tensions.[39−46] However, this invocation of macroscopic parameters limits applications of SPT to study the subtle changes due to temperature and pressure, for example, that are closely associated with the molecule-scale properties. A thoroughly molecular theory was developed by Pratt and Chandler (PC),[47] based on the theory of simple liquids. The PC theory invokes radial correlation functions in the context of Ornstein−Zernike

integral equations with appropriate closures. Lazaridis and Paulaitis[48] (LP) use an expansion of the conformational entropy in terms of particle distribution functions. Both PC and LP theories relate the structural ordering of water by the nonpolar solute to the hydration thermodynamics through solute−water pair correlations.
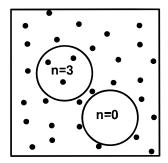
Probably the most powerful approach is the direct computer simulation of hydrophobic hydration phenomena using molecular dynamics or Monte Carlo methods.[49] Computer simulations are flexible and, with the advent of ever faster computers, the system size and time scale limitations are becoming less of a concern. However, the *interpretation* of computer simulation results necessitates a well-founded theoretical framework. Here, and in the aforementioned theories, computer simulations provide critical input that is not readily available from experiments.

The theoretical approach pursued here describes hydrophobic hydration and hydrophobic interactions using chemical potentials of the simplest hydrophobic solutes in water−"hard" molecules exerting entirely repulsive interactions on water molecules. The solvation chemical potentials for hard-core solutes are directly related to the presence of cavity volumes of molecular size due to density fluctuations in bulk water. We quantify these density fluctuations using an approach motivated by information theory (IT).[50] From a maximum-entropy principle,[51] we find the "best-possible" description of the fluctuations that satisfies certain experimental constraints. The virtues of such an approach are its simplicity, efficiency, and accuracy for molecule-size solutes. In addition, the IT model expresses the simple hydrophobic phenomena using properties of bulk water alone. This allows us to relate hydrophobic effects to the peculiar properties of water that distinguishes it from nonpolar solvents. The IT model builds on concepts introduced in SPT, specifically the relation between the probability of finding a molecule-size cavity in water and the chemical potential of solvation of hard particles. In its simplest form, the IT model is also related to Ornstein−Zernike integral equation theories and the PC theory.[50,52−54]

The paper is organized as follows: After developing the IT model for hard nonpolar solutes and a generalization to continuous solute−solvent interactions, we will discuss practical aspects of the implementation. Limitations in the macroscopic limit will be analyzed before we view the IT model from a historical perspective. We will then present results for the simplest hydrophobic effects: solvation of spherical solutes, methane−methane interaction in water, and contributions to the torsional equilibrium of butane. The temperature dependence of hydrophobic hydration and the entropy convergence will be studied subsequently. We will then quantify the effects of pressure on hydrophobic interactions, leading to a model for the pressure denaturation of proteins. The effects of salt on hydrophobic hydration will be discussed briefly. We will also introduce a recently developed perturbation theory model[55] based on the energetic loss of water molecules at the solute−water interface. This model allows us to extend our analysis of hydrophobic effects further to mesoscopic and macroscopic solutes. We will conclude with an attempt to give answers to the question how water differs from hydrocarbon liquids as a solvent for nonpolar solutes.

II. Information Theory Model of Hydrophobic Hydration

Simple Hydrophobic Effects: Thermodynamics of Dissolving a Hard Particle in Water. The simplest hydrophobic solute is a cavity or, equivalently, a hard-core particle which excludes water-oxygen atoms from a volume v of a given shape

Feature Article

J. Phys. Chem. B, Vol. 102, No. 51, 1998 **10471**

Figure 1. Schematic two-dimensional representation of the probabilities p_n of observing n solvent centers inside a randomly positioned volume v in the bulk fluid. Two cases are shown: A successful insertion with $n = 0$ that would contribute to p_0, and an insertion with $n = 3$ contributing to p_3.

and molecular size. Cavity formation constitutes the important, first step in solvating any nonpolar solute in water.[56] The solvation thermodynamics of a hard particle is determined by the excess chemical potential μ^{ex} corresponding to the free energy of its transfer from an ideal gas into the aqueous environment. Statistical mechanics relates this excess chemical potential to the probability p_0 of finding an empty volume v in water, i.e., a cavity of a given size and shape[36]

$$\mu^{ex} = -k_B T \ln p_0 \qquad (1)$$

To determine the chemical potential μ^{ex}, we need to quantify the probability p_0 of successfully inserting a hard-core solute of a given size and shape into equilibrium conformations of water, as illustrated in Figure 1. A virtue of such an approach is that the solvation thermodynamics characterized by μ^{ex} is determined by the properties of pure water, with the solute entering through its molecular volume v.

b. Information Theory Approach to Excess Chemical Potentials of Solvation. The goal is to estimate accurately the probability p_0 that a given hard-core solute inserted into water does not overlap with any of the solvent centers, defined as the positions of water-oxygen atoms. The IT approach does not attempt to model this quantity directly. Instead, it focuses on the set of probabilities p_n of finding n water-oxygen atoms inside the observation volume, with p_0 being just one of the p_n. We will attempt to get accurate estimates of the p_n, and p_0 in particular, using experimentally available information as constraints on the p_n. The moments of the fluctuations in the number of solvent centers within the observation volume v provide such constraints.

For a given observation volume v in bulk water, the moments of the fluctuations in the particle number n are determined from the p_n as follows:

$$\langle n^k \rangle = \sum_{n=0}^{\infty} p_n n^k \qquad (2)$$

where $\langle \cdots \rangle$ denotes a thermal average. The zeroth, first, and second moment can be expressed in terms of experimentally accessible quantities:

$$\langle 1 \rangle = \sum_{n=0}^{\infty} p_n = 1 \qquad (3a)$$

$$\langle n \rangle = \sum_{n=0}^{\infty} p_n n = \rho v \qquad (3b)$$

$$\langle n^2 \rangle = \sum_{n=0}^{\infty} p_n n^2 = \langle n \rangle + \rho^2 \int_v d\mathbf{r} \int_v d\mathbf{r'} \, g(|\mathbf{r} - \mathbf{r'}|) \qquad (3c)$$

where ρ is the number density of bulk water and $g(r)$ is the radial distribution function between water-oxygen atoms in bulk water, which can be determined from X-ray or neutron-scattering measurements or computer simulations. These moment conditions provide constraints on the p_n's, and guarantee that the p_n are normalized and have the correct first and second moments. Higher moments would require knowledge of triplet and higher order correlation functions which are not generally accessible to experiments, but can be calculated from computer simulations.[58]

The IT approach attempts to provide the "best-possible" estimate of the probabilities p_n under the constraints of the available information,[51] defined as the set $\{p_n\}$ that maximizes an information entropy η subject to the information constraints

$$\max_{\{constraints\}} \eta(\{p_n\}) \qquad (4)$$

In the most general form, we adopt a relative or cross entropy,[59]

$$\eta(\{p_n\}) = - \sum_{n=0}^{\infty} p_n \ln \left(\frac{p_n}{\hat{p}_n} \right) \qquad (5)$$

where $\hat{p}_n$ represents an empirically chosen "default model."

We consider two natural choices of default models: the Gibbs default model $\hat{p}_n \propto 1/n!$, which leads to a Poisson distribution for a given mean, as would be expected for an ideal gas, and a flat distribution ($\hat{p}_n = 1$ for $n \leq n_{max}$ and $\hat{p}_n = 0$ otherwise), which results in a discrete Gaussian form of p_n with given mean and variance. Empirically, we find that the latter choice is accurately applicable to molecule-size cavities.[50]

Maximizing the information entropy under the constraints of eq 3 leads to

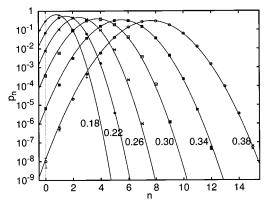$$p_n = \hat{p}_n e^{\lambda_0 + \lambda_1 n + \lambda_2 n^2} \qquad (6)$$

where λ_0, λ_1, and λ_2 are the Lagrange multipliers chosen to satisfy the moment conditions eq 3.

Figure 2 shows p_n distributions for spherical observation volumes v calculated from computer simulations of SPC[57] water.[50] The solute exclusion volume is defined by the distance d of closest approach of water-oxygen atoms to the center of the sphere. For the range of solute sizes studied, we find that $\ln p_n$ values are closely parabolic in n. This would be predicted from the flat default model with $n_{max} \rightarrow \infty$, as shown in Figure 2.
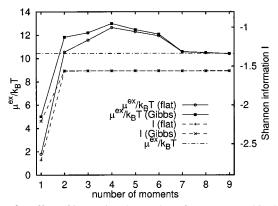
Figure 3 illustrates the effect of including higher moments in the IT model. Results are shown both for the Gibbs and the flat default models. We find that the prediction of μ^{ex} is greatly improved when the second moment (i.e., the variance of the particle number) is included in addition to the mean. However, inclusion of higher moments initially makes the prediction worse. Only when seven or more moments are used is the prediction as accurate as the two-moment model. Also shown in Figure 3 is the calculated Shannon information $I(\{p_n\})$

$$I(\{p_n\}) = \sum_{n=0}^{\infty} p_n \ln p_n \qquad (7)$$

Including the second moment results in a large gain in information, whereas the gains upon including additional higher

Figure 2. Probabilities p_n for observing n water-oxygen atoms in spherical cavity volumes.[50] Results from Monte Carlo simulations of SPC water[57] are shown as symbols. The parabolas are the predictions of the flat default model of the IT approach. The center-to-center exclusion distance d (in nanometers) is noted next to the curves.

Figure 3. Effect of increasing the number of moments used in the IT calculations. Shown as a function of the number of moments is the predicted excess chemical potential of a methane-size hard sphere with exclusion radius $d = 0.33$ nm for solvation in SPC/E water[60] (left-hand scale). Also shown for reference is the actual chemical potential (dotted-dashed line). The Shannon information I (right-hand scale) illustrates that the third and higher moments do not result in an appreciable gain in information.

moments are small: moments of order three and higher are, in this respect, "uninformative," as measured by the gain in Shannon information $I(\{p_n\})$ (see also ref 61). Those higher moments do not significantly alter the estimated values of p_0 and μ^{ex} for the solute-size range considered in Figures 2 and 3.

c. Continuous Information Theory. A more general statement of the principles underlying the IT approach follows from a generalization to continuous interactions between the solvent and the hydrophobic solute. Such a generalization can be achieved by explicitly considering solvent positions within a microscopic volume, in addition to the occupancy numbers considered in the basic IT approach. We define probability distributions $p(j; \mathbf{r}_1, ..., \mathbf{r}_j)$ of observing exactly j particles within the observation volume v at positions $\mathbf{r}_1, ..., \mathbf{r}_j$ in infinitesimal volume elements $d\mathbf{r}_1, ..., d\mathbf{r}_j$. The $p(j; \mathbf{r}_1, ..., \mathbf{r}_j)$ allow us to calculate solvation chemical potentials of a solute with continuous interactions $u(\mathbf{r}_1, \mathbf{r}_2, ...)$ between solvent molecules at positions $\mathbf{r}_1, \mathbf{r}_2, ...$ and a solute at the origin. Within the observation volume v, the solute−solvent interactions are treated explicitly. Finite-range interactions provide a natural choice for v; otherwise, a finite volume v can be chosen with corrections for long-range interactions.

Widom's formula[62] relates the excess chemical potential of the solute μ^{ex} to the normalized $p(j; \mathbf{r}_1, ..., \mathbf{r}_j)$

$$e^{-\beta\mu^{ex}} = \langle e^{-\beta u(\mathbf{r}_1, \mathbf{r}_2, ...)} \rangle$$

$$= \sum_j [\prod_{i=1}^{i=j} \int_v d\mathbf{r}_i] \, p(j; \mathbf{r}_1, ..., \mathbf{r}_j) e^{-\beta u(\mathbf{r}_1, ..., \mathbf{r}_j)} \quad (8)$$

where $\beta^{-1} = k_B T$.

Calculating $p(j; \mathbf{r}_1, ..., \mathbf{r}_j)$ directly would require knowledge of higher order correlation functions. Instead, our goal is to infer the $p(j; \mathbf{r}_1, ..., \mathbf{r}_j)$ from available information, such as the one- and two-particle densities in the observation volume v, expressed as constraint functionals:

$$\rho(\mathbf{r}) = \sum_\alpha \langle \delta(\mathbf{r} - \mathbf{r}_\alpha) \rangle$$

$$= \sum_{j \geq 1} \binom{j}{1} [\prod_{i=1}^{i=j} \int_v d\mathbf{r}_i] \, \delta(\mathbf{r} - \mathbf{r}_1) p(j; \mathbf{r}_1, ..., \mathbf{r}_j) \quad (9a)$$

$$\rho^2 g^{(2)}(\mathbf{r}, \mathbf{r}')/2 = \langle \sum_{\alpha > \gamma} \delta(\mathbf{r} - \mathbf{r}_\alpha) \delta(\mathbf{r}' - \mathbf{r}_\gamma) \rangle$$

$$= \sum_{j \geq 2} \binom{j}{2} [\prod_{i=1}^{i=j} \int_v d\mathbf{r}_i] \, \delta(\mathbf{r} - \mathbf{r}_1) \delta(\mathbf{r} - \mathbf{r}_2) p(j; \mathbf{r}_1, ..., \mathbf{r}_j)$$

$$(9b)$$

where $\mathbf{r}$ and $\mathbf{r}'$ are positions inside the observation volume v. For a homogeneous fluid, the density will be uniform, i.e., $\rho(\mathbf{r})$ will be independent of position; and the two-particle density distribution will be the radial distribution function of the homogeneous system, $g^{(2)}(\mathbf{r}, \mathbf{r}') = g(|\mathbf{r} - \mathbf{r}'|)$.

In analogy to eq 5, we define an information entropy η for continuous solvent positions and discrete occupancy numbers[63]

$$\eta \equiv -\sum_j [\prod_{i=1}^{i=j} \int_v d\mathbf{r}_i] \, p(j; \mathbf{r}_1, ..., \mathbf{r}_j) \ln[v^j j! p(j; \mathbf{r}_1, ..., \mathbf{r}_j)]$$

$$(10)$$

We include the factor of v^j in the logarithm of eq 10 for dimensional consistency. Maximizing this entropy functional under the constraints of eq 9 results in an expression for the probability distribution $p(j; \mathbf{r}_1, ..., \mathbf{r}_j)$

$$-\beta^{-1} \ln[v^j j! p(j; \mathbf{r}_1, ..., \mathbf{r}_j)] =$$

$$\sum_{k=1}^{j} \omega^{(1)}(\mathbf{r}_k) + \frac{1}{2} \sum_{k,l=1}^{j} \omega^{(2)}(\mathbf{r}_k, \mathbf{r}_l) \quad (11)$$

The Lagrange multipliers $\omega^{(1)}(\mathbf{r}_k)$ and $\omega^{(2)}(\mathbf{r}_k, \mathbf{r}_l)$ are chosen such that the $p(j; \mathbf{r}_1, ..., \mathbf{r}_j)$ satisfy the constraint functionals eq 9. Incorporating additional n-particle correlation information ($n > 2$) is straightforward. In a practical implementation, one can subdivide the observation volume into a finite number of volume elements. The constraint functionals, eq 9, then reduce to a finite number of constraints.

Note that the probability distributions $p(j; \mathbf{r}_1, ..., \mathbf{r}_j)$ have a Boltzmann−Gibbs structure, i.e., they are proportional to an exponential of effective interactions $\omega^{(1)}(\mathbf{r}_k)$ and $\omega^{(2)}(\mathbf{r}_k, \mathbf{r}_l)$ in $k_B T$ units, divided by $j!$. The summation and integration of the $p(j; \mathbf{r}_1, ..., \mathbf{r}_j)$ results in the familiar form of a grand-canonical partition function for a microscopic volume v embedded in a large bath of solvent molecules. The effective interactions entering the Boltzmann−Gibbs factors in this grand-canonical partition function are the Lagrange multipliers $\omega^{(1)}(\mathbf{r}_k)$ and $\omega^{(2)}(\mathbf{r}_k, \mathbf{r}_l)$. These effective interactions are chosen to satisfy available information constraints, rather than being derived directly from integrating out bath degrees of freedom.

Feature Article

J. Phys. Chem. B, Vol. 102, No. 51, 1998 **10473**

$\omega^{(1)}(\mathbf{r})$ is expected to be a spatial constant approximately the negative chemical potential of the solvent.[55] Similarly, $\omega^{(2)}(\mathbf{r}, \mathbf{r}')$ will be approximately an interatomic pair potential, except in a small region near the surface of the subsystem.

d. Some Practical Aspects of the Information Theory Model. Here, we provide details on the practical implementation of the IT model. Before discussing specific details, we note that the required moments of particle-number fluctuations can be obtained in situ from simulation data. This idea is most direct for a uniform liquid. The observation volume v is planted as a stencil in the simulation volume, and the required moments are extracted as averages over a set of simulation configurations. For a uniform liquid the positioning of the observation volume is irrelevant and many positions can be used simultaneously. It is worth noting further that since the occupation numbers can only be a finite number of nonnegative integers, only a finite number of binomial moments will be nonzero. Similar procedures apply to nonuniform systems, such as the solvation structure near a fixed solute, but the positioning of the observation volume is then relevant.

The observation volume may be subdivided into several strata. This introduces cross moments in the general case and permits conceptually interesting possibilities for modeling the probabilities. As an example, consider the mean density in a volume element external to a core region conditional on the requirement that the core region be empty. With such considerations, the IT modeling naturally produces a prediction of the hydration structure near a hydrophobic solute without special geometrical limitations. Such possibilities have scarcely been studied so far, however. For the calculation of the required moment information, stratification is no particular problem but it may affect the computational efficiency. Note, that a stratified representation can also be derived from coarse graining the continuous IT of section II.c.

Next, we will illustrate several methods to calculate the second moment of the particle-number fluctuations. Then we will describe numerical methods for the entropy maximization.

Calculation of Particle-Number Variances. The second-moment constraint eq 3c requires the calculation of a double integral over the volume v involving the distance-dependent pair correlation function $g(r)$. Such integrals can be evaluated using Monte Carlo techniques. The average of the pair correlation function $\langle g(|\mathbf{r} - \mathbf{r}'|) \rangle$ can be determined by placing two points $\mathbf{r}$ and $\mathbf{r}'$ randomly inside the volume v according to a uniform probability density. This average is then multiplied by the square of the volume v to give an estimate of the integral in eq 3c.

As suggested above, the variance and higher moments of particle-number fluctuations can be determined directly from molecular simulations. Unlike p_0, the mean and variance can be calculated accurately from insertion also for large solutes. Objects with volume v (shape and size) are inserted with random positions and orientations into water configurations taken from an equilibrium molecular dynamics or Monte Carlo simulation. The mean and variance of the particle number n is then determined directly.

Volumes of certain shapes are amenable to analytical evaluation. For spherical volumes v of radius d, Hill[64] derived a transformation of the six-dimensional integral to one-dimensional form. Such transformations can be accomplished by determining the pair-distance distribution $P(R)$ well-known from small-angle scattering theory[65]

$$P(R) = \int_v d\mathbf{r} \int_v d\mathbf{r}' \, \delta(R - |\mathbf{r} - \mathbf{r}'|) \quad (12)$$

where $\delta(x)$ is Dirac's delta function. This leads to the following expression for the second moment:

$$\langle n^2 \rangle = \langle n \rangle + \rho^2 \int dR \, P(R) g(R) \quad (13)$$

We can also use the three-dimensional analog to eq 12

$$P(\mathbf{R}) = \int_v d\mathbf{r} \int_v d\mathbf{r}' \, \delta[\mathbf{R} - (\mathbf{r} - \mathbf{r}')] \quad (14)$$

Fourier transformation relates $P(\mathbf{R})$ to the form factor $S(\mathbf{k})$ of the volume v

$$\tilde{P}(\mathbf{k}) = \int d\mathbf{r} P(\mathbf{r}) \, e^{i\mathbf{k}\cdot\mathbf{r}} = |S(\mathbf{k})|^2 \quad (15)$$

where

$$S(\mathbf{k}) = \int_v d\mathbf{r} e^{i\mathbf{k}\cdot\mathbf{r}} \quad (16)$$

The Fourier transform eq 15 can be inverted as

$$P(\mathbf{R}) = \frac{1}{(2\pi)^3} \int d\mathbf{k} \tilde{P}(\mathbf{k}) e^{-i\mathbf{k}\cdot\mathbf{r}} \quad (17)$$

As a generalization of Hill's result for a single sphere[64] we find for a collection of N nonoverlapping spheres of radius d

$$P(R) = 4\pi R^2 \left\{ \left[N\pi d^3 \left(\frac{4}{3} - \frac{R}{d} + \frac{R^3}{12d^3} \right) \right] \theta(2d - R) + \right.$$

$$\sum_{i=1}^{N-1} \sum_{j=i+1}^{N} \left[\pi d^3 \left(\frac{4}{3}(1 - x_{ij}) - \frac{y_{ij}^{3/2} - |R - r_{ij}|^3}{3r_{ij}Rd} \right. \right. +$$

$$\left. \left. \frac{y_{ij}^{5/2} - |R - r_{ij}|^5}{60r_{ij}Rd^3} \right) \right] \theta[R - (r_{ij} - 2d)]\theta(r_{ij} + 2d - R) \right\} \quad (18)$$

where r_{ij} is the distance of the centers of spheres i and j, $x_{ij} = (R^2 + r_{ij}^2 - 4d^2)/(2Rr_{ij})$, and $y_{ij} = R^2 + r_{ij}^2 - 2Rr_{ij}x_{ij}$. Using this method, analytical results can also be found for rotation ellipsoids with axes $a = b$ and c.

Maximizing the Information Entropy. Maximization of the information entropy eq 5 is easily performed using Lagrange multipliers for the constraints. For constraints on mean and variance, this leads to the expression eq 6 for p_n. Lagrange multipliers λ_0, λ_1, and λ_2 are then calculated such that the corresponding p_n satisfy the moment conditions eq 3. This corresponds to solving three nonlinear equations with three unknowns which can be accomplished, for instance, by using a Newton−Raphson method. Alternatively, one can use standard minimization packages, minimizing the squared differences of the left- and right-hand sides of the moment constraint equations. This is consistent with the idea of minimizing the "thermodynamic potential"

$$f(\lambda_1, ..., \lambda_{k_{max}}) \equiv \ln\left[1 + \sum_{j=1}^{k_{max}} \hat{p}_j \exp\left(-\sum_{k=1}^{k_{max}} \lambda_k \binom{j}{k} \right) \right] +$$

$$\sum_{k=1}^{k_{max}} \lambda_k \left\langle \left\langle \binom{j}{k} \right\rangle \right\rangle \quad (19)$$

here expressed in terms of the binomial moment information and for a general default model.

e. Some Pitfalls of the Simplest Models. It is a helpful, heuristic view that the IT approach studies a model grand

partition function associated with a molecular scale volume and involving effective interactions. Because this may be an unusual setting for the consequent statistical thermodynamic calculations, conventional results are not guaranteed. Here we note some of the pitfalls that have been encountered for the simplest models. These discussions emphasize that the orientation for development of this approach is to discover models that work.

Nonseparability of Chemical Potentials of Distant Sites within a Gaussian Model. Consider two spheres of exclusion radius λ separated by a distance large compared to λ. The excess chemical potential of the two spheres *should be* 2 times that of the individual spheres $\mu^{ex}(1, 2) = 2\mu^{ex}$. The mean and variance of the particle-number fluctuations are also additive. For the combined volume, we will have $m_2 = 2m_1$ and $\sigma_2^2 = 2\sigma_1^2$, where m_i and σ_i^2 are the means and variances of the particle-number distributions of an individual sphere ($i = 1$) and the two spheres ($i = 2$). Following the flat default model, we approximate p_0 by a Gaussian form[14]

$$p_0 \approx \frac{e^{-m_i^2/2\sigma_i^2}}{\sqrt{(2\pi\sigma_i^2)}} \qquad (20)$$

We then find that the corresponding chemical potential of an infinitely distant pair of spheres is not exactly that of two individual spheres

$$\mu^{ex}(1, 2) - 2\mu^{ex} \approx -\frac{k_BT}{2}\ln(\pi\sigma_1^2) \qquad (21)$$

This nonadditivity is a direct consequence of the Gaussian model and can be simply repaired by insisting accurately on zero probability for negative occupancies. In fact, the definition of our problem here requires that the occupancies be nonnegative integers.

Additivity can be recovered by dividing the two sphere volume into two strata: one for each sphere or, when the spheres overlap, the individual strata can be defined by utilizing the plane of intersection of the spherical surfaces as a bounding surface. Suppose again that the spheres are far apart and that the probability of occupancy of one sphere is independent of the occupancy of the other. The cross correlation between the numbers n_1 and n_2 of solvent centers in the two nonoverlapping strata is then given by

$$\langle n_1 n_2 \rangle = \rho^2 \int_{v_1} d\mathbf{r}_1 \int_{v_2} d\mathbf{r}_2 g(|\mathbf{r}_1 - \mathbf{r}_2|)$$
$$= \rho^2 v_1 v_2 = \langle n_1 \rangle\langle n_2 \rangle \qquad (22)$$

corresponding to *uncorrelated* particle-number fluctuations. An expanded IT model uses the joint probabilities $p(n_1, n_2)$ of finding n_1 particles in v_1 and n_2 particles in v_2. Including the constraint eq 22 derived from stratification in that expanded IT model gives the correct result that the hydration free energy of the two spheres is the sum of the hydration free energies of the individual spheres.

The nonadditivity in the simple model is caused by the possibility of having a zero occupancy of the volume v with a *negative* number $-n$ of particles in subvolume v_1 that is compensated by a positive number n of particles in subvolume v_2. By imposing explicitly that each of the subvolumes has zero occupancy when the total occupancy is zero, the nonadditivity is eliminated. This argument illustrates that the restriction of the probabilities p_n to nonnegative integers can be significant. This example also emphasizes that arguments well

justified about the center of a distribution can lead to fundamental errors when applied to the wings of a distribution.

Macroscopic Limit. For the flat default model, we can calculate the limit of large solutes. The variance in the particle number is then given by the isothermal compressibility χ_T,

$$\frac{\langle n^2 \rangle - \langle n \rangle^2}{\langle n \rangle} = \rho k_BT\chi_T \text{ for } v \to \infty \qquad (23)$$

For the flat default model and a spherical solute with exclusion radius λ, we find that the chemical potential grows with the volume of the solute

$$\frac{\partial\mu}{\partial\lambda} \approx \frac{2\pi\lambda^2}{\chi_T} \qquad (24)$$

where we used the Gaussian approximation eq 20. The flat default model predicts for the water density $\rho G(\infty)$ at contact with a hard wall:

$$G(\infty) = \lim_{\lambda\to\infty} (4\pi\lambda^2 \rho k_BT)^{-1} \frac{\partial\mu}{\partial\lambda} \approx (2\rho k_BT\chi_T)^{-1} \qquad (25)$$

which for water under standard conditions results in $G(\infty) \approx 8$. The contact value for a flat wall, however, is well-known to be $G(\infty) = p/\rho k_BT$, where p is the pressure. If we use bulk density and pressure of water under standard conditions, we obtain $p/\rho k_BT \approx 7.4 \times 10^{-4}$; for saturated water vapor,[38] we find $p/\rho k_BT \approx 2 \times 10^{-5}$. Clearly, the contact value at a flat wall $G(\infty)$ would be grossly overestimated if the flat default model were used in this macroscopic limit.

In the limit of large solutes we expect the multiphasic nature of water to become important. Stillinger[38] pointed out that the solvation of hard spheres much larger than a water molecule can be quantified by considering that a molecularly thick vapor layer surrounds the solute. For large solutes, the formation of a correspondingly large water-vapor bubble with subsequent insertion into that bubble will cost less free energy than inserting directly into the *liquid* phase. The simplest IT model uses a flat or Gibbs default model and does not account for this possibility, as density fluctuations are of either Gaussian or Poisson-like character, respectively. More elaborate default models should however be able to account for the possibility of vaporizing a certain small volume. But clearly, defining such models would require knowledge about the free energy of microscopic vapor-bubble formation which is a task as formidable as the calculation of solvation chemical potentials.

An indication of the large-solute effects can already be seen in Figure 2. For solutes of size $d = 0.3$ nm and larger, we find that p_1 is depressed relative to the flat default model. This means that it is relatively less likely to find an isolated water molecule in a cavity than would be predicted from that simple model. On the basis of the foregoing discussion, for solutes of increasing size we expect that p_0 will be become larger than predicted from the flat default model.

f. Historical Perspective. *Scaled Particle Theory Ideas.* The IT approach can be viewed in the context of preceding studies of the insertion probability p_0. Mayer and Montroll[66] and later Reiss et al.[36] expressed p_0 in terms of higher order correlation functions of the bulk fluid,

$$p_0 = 1 + \sum_{m=1}^{\infty} \frac{(-1)^m}{m!} \int_v d\mathbf{r}_1 \int_v d\mathbf{r}_2 \ldots$$
$$\int_v d\mathbf{r}_m \rho^m g^{(m)}(\mathbf{r}_1, \mathbf{r}_2, ..., \mathbf{r}_m) \qquad (26)$$

Feature Article

J. Phys. Chem. B, Vol. 102, No. 51, 1998 **10475**

where $\rho^m g^{(m)}$ is the m-body joint density for solvent centers (here, water–oxygen atoms). These are standard combinatorial results, more frequently seen in forms such as[67]

$$p_0 = 1 + \sum_{m=1}^{\infty} (-1)^m \left\langle\!\!\left(\!\! \binom{n}{m} \!\!\right)\!\!\right\rangle \qquad (27)$$

and

$$p_j = \sum_{m=0}^{\infty} (-1)^m \binom{j+m}{j} \left\langle\!\!\left(\!\! \binom{n}{j+m} \!\!\right)\!\!\right\rangle \qquad (28)$$

where n is the number of solvent centers within υ. The first of these can be derived directly by noting that $p_0 = \langle(-1 + 1)^n\rangle$ where $(-1 + 1)^n$ is an indicator function that is one for $n = 0$ and zero otherwise. These sums truncate sharply if only a finite maximum number of particles can be present in the observation volume. They are of practical value for small volumes where the maximum number of solvent centers that can possibly occupy that volume is small. For larger volumes, large terms of alternating sign appear in the expansion eq 27 that make it difficult to use estimated values for the factorial moments in this linear fashion.

Equating the excess chemical potential μ^{ex} to the quasi-static work of creating a cavity results in an expression for p_0 in terms of the contact value $G(\lambda)$ of the solvent density at the surface of the exclusion volume υ. For a spherical exclusion volume of radius λ we have.[36,68]

$$\mu^{\text{ex}} = -k_{\text{B}}T \ln p_0 = 4\pi\rho k_{\text{B}}T \int_0^d G(\lambda)\lambda^2 d\lambda \qquad (29)$$
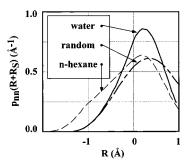
This result is formally exact for a hard-sphere solute and establishes that $4\pi\rho k_{\text{B}}TG(\lambda)\lambda^2$ is the compressive force exerted by the solvent on a hard spherical solute of diameter λ. If the solvent is considered to contain a hard core itself, there is a maximum number of solvent particles n_{max} that can occupy a certain volume υ. This results in useful, exact expressions for the case of $n_{\text{max}} = 1$ and 2. For larger solutes, the expected macroscopic solvation behavior[37,38]

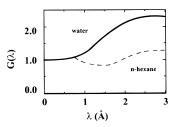$$\mu^{\text{ex}} \sim p(4\pi\lambda^3/3) + \gamma(4\pi\lambda^2) \qquad (30)$$

is used as a basis for extrapolation. Here p is the pressure and γ is the liquid–vapor surface tension. In the intermediate molecular region, the approximate asymptotic form is connected smoothly to the exact curve for small solutes.[37,38]

Computer Simulation Studies. The cavity formation probability p_0 lends itself to direct computer simulation studies by test-particle insertion. Spherical volumes υ in water were studied extensively using computer simulations.[69-74] Similar insertion methods were also used to study polymer solubilities.[75] The simulation studies of Pohorille and Pratt[69-71] clarified a number of interesting speculations on hydrophobicity and provided the first discriminating tests of theoretical models for $G(\lambda)$.

One hypothesis that has sparked interest in recent years is the idea that the low solubility of inert gases in liquid water is due to the small size of the water molecule and, consequently, the "interstitial" cavities will be smaller in water than in coexisting organic liquids of common interest.[76,77] Since the present work deals directly with such cavities, it is straightforward to test that idea. Figure 4 shows distributions[71] of the distances from an arbitrary point to the nearest interaction site for three cases of interest: liquid *n*-hexane, liquid water, and

Figure 4. Distributions p_{nn} of the distance $R + R_S$ from a random point to the nearest neighboring site in water, *n*-hexane, and an ideal gas with water density.[71] R_S is the van der Waals radius of the solvent. For each of the three fluids, the solvent van der Waals volumes are represented by a superposition of spherical sites of one type only. The ideal-gas curve is the Hertz distribution $4\pi\rho(R + R_S)^2 \exp[-4\pi\rho(R + R_S)^3/3]$ with ρ the molecular (or oxygen) density of liquid water at 301 K and atmospheric pressure. The van der Waals radius of water oxygen is $R_S = 1.35$ Å; that of united-atom carbons in *n*-hexane is $R_S = 1.85$ Å.
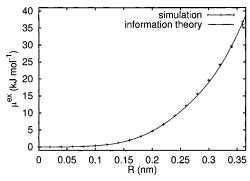
Figure 5. Contact densities $G(\lambda)$ of water and *n*-hexane at the surface of hard-sphere solutes.[69] $G(\lambda)$ gives the compressive force of the solvent on a hard spherical solute.

an ideal gas with water density. Reasonable and customary values are used for the van der Waals radii of the solvent interaction sites in each case. Figure 4 shows that the most probable cavity radii are quite small in all those cases as is expected for liquids. Also, the difference in the most probable cavity size between liquid *n*-hexane and liquid water is not large and smaller than the corresponding difference between liquid water and an ideal gas with water density. The fact that the differences seen here are slight is, presumably, defined by the fact that the most basic units considered in *n*-hexane are the methyl and methylene groups. These are not so different in size from a water molecule. In contrast, simple equation of state models might treat the *n*-hexane molecule as a sphere of substantially larger size. It can also be noted that, on a packing fraction basis, typical organic liquids are denser than liquid water.[70]

One feature in Figure 4 that does distinguish water is the breadth of the distributions. The distribution of the nearest solvent site neighboring an arbitrary position in the liquid is *narrower* in liquid water. The widths of these distributions are independent of the van der Waals radii assigned to the solvent sites. The interpretation is that, compared to other liquids, water is "stiffer" when larger cavities must be opened.

This comparative stiffness can be analyzed further by determining the contact functions $G(\lambda)$ for water and hydrocarbon liquids and comparing the compressive force that such solvents exert on a hard spherical solute. As shown in Figure 5, water exerts a higher compressive force on such a solute than typical hydrocarbon solvents. It is thus an accurate view on molecular-scale hydrophobic effects that water "squeezes-out" hydrophobic solutes.[78,79]

Field Theory Models. A perspective related to the IT approach pursued here has been adopted before by Chandler.[52]

Figure 6. Excess chemical potential of hard-sphere solutes in SPC water[57] as a function of the exclusion radius d. The symbols are simulation results, compared with the IT prediction using the flat default model (solid line).[50]

Equilibrium fluctuations of the water density are approximated by a Gaussian model. The partition functions are then calculated for the two systems with and without a cavity of volume v present, using a field-theoretical method. Chandler then shows that this continuous Gaussian fluctuation model leads to the Pratt−Chandler integral equation theory.[47] For sufficiently large volumes, a Gaussian field model is expected to reproduce accurately the p_n if the continuous probability densities of particle numbers are mapped to discrete values of n and the negative values of n are disregarded.
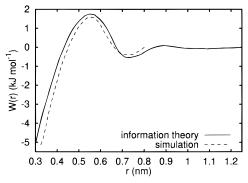
III. Results for Elementary Hydrophobic Effects

a. Hydration of Simple Spherical Solutes. The probabilities p_n of observing exactly n oxygen centers inside spherical volumes, shown in Figure 2, are reproduced accurately using IT with a flat default model. The corresponding excess chemical potentials of hydration of those solutes, $\mu^{ex} = -k_B T \ln p_0$, are shown in Figure 6.[50] As expected, μ^{ex} increases with increasing cavity radius. The agreement between IT predictions and computer simulation results is excellent over the whole range $d \leq 0.36$ nm accessible to direct simulation calculations of p_0.
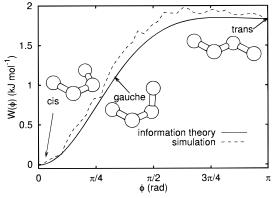
b. Methane−Methane Potential of Mean Force (PMF). We now focus on the simplest model of hydrophobic interactions exemplified by the free energy of bringing together two methane-size cavities in water.[47,49,80−85] This free energy profile defines a PMF. We obtain the cavity contribution to the methane−methane PMF by calculating the excess chemical potential $\mu^{ex}(r)$ of a cavity volume described by two spheres each of radius d and separated by a distance r. The PMF is then defined as $W(r) = \mu^{ex}(r) - \lim_{s\to\infty} \mu^{ex}(s)$. This definition guarantees that $W(r) \to 0$ for $r \to \infty$, avoiding the problem of nonadditivity discussed above for nonstratified volumes.

Figure 7 shows a comparison of the cavity PMF calculated using IT with that obtained from explicit simulations by Smith and Haymet.[81] The flat default model has been used here and throughout this paper, unless otherwise noted. Also, an exclusion radius of $d = 0.33$ nm has been used for methane-size cavities corresponding to a distance where the methane−water oxygen radial distribution function reaches a value of 1.0 in commonly used models.[86,87] The direct interaction between the two methane molecules has been subtracted from the simulation PMF to get approximately the cavity contribution to the methane−methane PMF.

In agreement with the simulation data, the PMF calculated using IT shows features characteristic of hydrophobic interactions. A free energy minimum is observed corresponding to overlapping hard spheres. That deep minimum is separated by a barrier from a second minimum at a distance of about 0.7

Figure 7. PMF between two methane-size cavities in SPC water,[57] comparing explicit computer simulations[81] (dashed line) with the IT prediction[50] (solid line). Note that the simulation curve is based on continuous solute−solvent interactions, subtracting the methane−methane interaction potential from the methane−methane PMF.

Figure 8. Water contribution to the torsional PMF of butane from IT[50] and explicit computer simulation[88] (dashed line).

nm. The second minimum corresponds to solvent-separated pairs of methane-size cavities. In addition, we observe a third shallow minimum which was also seen in computer simulations by Lüdemann et al.[85] The equilibrium between the solvent-separated and contact minimum as a function of pressure provides insights into pressure denaturation of proteins, as described in section V.
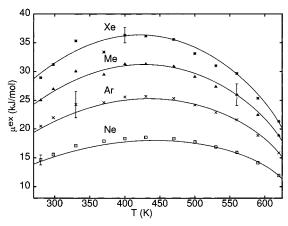
c. Solvent Contributions to the Torsional Equilibrium of Butane. As a final example of a simple hydrophobic effect, Figure 8 shows the cavity contribution to the torsional PMF for n-butane in water. IT calculations are compared with explicit computer simulations by Beglov and Roux.[88] We find that the cavity PMF favors the compact cis ($\phi = 0$) structure over the extended trans structure by about 1.8 kJ/mol. The gauche structure ($\phi = \pi/3$) is favored over trans by about 0.7 kJ/mol. Those differences and the overall cavity PMF for the torsional isomerization of butane are in excellent agreement with the simulation data.

IV. Temperature Dependence of Hydrophobic Hydration

a. Solvation Chemical Potentials. The hydrophobic effect is often associated with characteristic temperature dependences.[11,89] One of the more astonishing observations is that the entropies of transfer of nonpolar molecules from gas phase or a nonpolar solvent into water converge at a temperature of about 400 K to approximately zero entropy change. Similar behavior was also seen in microcalorimetry experiments on unfolding of several globular proteins.[6−8] This analogy to the transfer data supported the hydrophobic-core model of protein folding: during unfolding predominantly nonpolar residues are transferred from a mostly nonpolar protein core into an aqueous environment.

Feature Article

J. Phys. Chem. B, Vol. 102, No. 51, 1998 **10477**

Figure 9. Chemical potential of hard-sphere solutes with exclusion radii corresponding to neon, argon, methane, and xenon as a function of temperature along the saturation curve of water.[14] The solid line is the IT prediction. The symbols are computer simulation data from insertion. Both simulation and theory data are for the SPC water[57] model.

We have used the IT model to clarify the molecular origin and the quantitative details of this striking entropy-convergence behavior.[14] Computer simulations were carried out to calculate the water-oxygen radial distribution function $g(r)$ at several temperatures along the experimental saturation curve of water. The $g(r)$'s together with the corresponding water densities are used as input in the IT model to calculate chemical potentials of hydration for hard solutes. Solute sizes of $d = 0.28$, 0.31, 0.33, and 0.345 nm were considered, corresponding approximately to neon, argon, methane, and xenon, respectively.

Figure 9 shows the chemical potentials for each of the spherical solutes as a function of temperature T, for T between 275 and 625 K. Also shown are the results of direct simulation calculations using test-particle insertion together with representative statistical errors. We find excellent agreement between simulation and theory for the chemical potentials over the whole temperature range. The chemical potentials are approximately parabolic except at the highest temperatures, and the curves for different solute sizes are shifted vertically with the maximum at about 400 K.
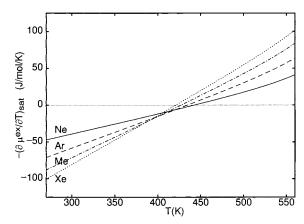
We obtain a solvation entropy by taking the derivative of the chemical potential along the saturation curve,

$$S_{sat} = -\left(\frac{\partial \mu^{ex}}{\partial T}\right)_{sat} \qquad (31)$$

Additional equation-of-state contributions to the standard solvation entropy are negligible, estimated to be less than 1 and 10 J/(mol K) for temperatures $T < 450$ and $T < 550$ K, respectively. Figure 10 shows the temperature dependence of the entropy S_{sat} for the different solutes. The entropies are large and negative at room temperature for all the solutes and decrease in magnitude with increasing temperature. The temperature dependence of entropies is approximately linear with slopes increasing with the increasing solute size. The resulting heat capacity

$$C_{sat} = T\left(\frac{\partial S_{sat}}{\partial T}\right)_{sat} \qquad (32)$$

is large and positive (approximately 40 cal mol^{-1} K^{-1} for a methane-size cavity). Moreover, the entropies converge at about 400 K to approximately zero entropy, although at closer inspection the temperature range of the convergence region is

Figure 10. Hydration entropy of hard-sphere solutes with exclusion radii corresponding to neon, argon, methane, and krypton as a function of temperature along the saturation curve of water.[14] Shown is the entropy defined in eq 31.

several 10 K and the entropy is not exactly zero at convergence. To understand the origin of this approximate convergence we determine in the following the factors entering into the IT model.

b. Origin of Entropy Convergence in Hydrophobic Hydration and Protein Folding. To quantify the different factors contributing to the entropy convergence,[14] we use the approximate Gaussian representation eq 20 for p_0 with mean $m = \langle n \rangle = \rho v$ and variance $\sigma^2 = \langle n^2 \rangle - \langle n \rangle^2$. This results in an estimate of the chemical potential,
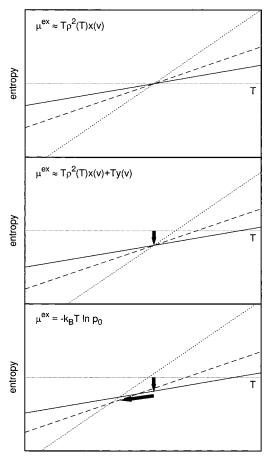
$$\mu^{ex} \approx T\rho^2\{k_B v^2/2\sigma^2\} + T\{k_B \ln(2\pi\sigma^2)/2\} \qquad (33)$$

The second term is smaller than the first and depends only logarithmically on the solute size. The solvation chemical potential may therefore be lowered by lowering the product of temperature and density $T\rho^2(T)$ or by increasing the particle-number fluctuations σ^2. The temperature dependence of $T\rho^2(T)$ along the saturation curve is nonmonotonic. On the other hand, we find that the variance $\sigma^2(T, v)$ changes only little over the range of temperatures in Figure 9.[14] Accordingly, we can approximate the chemical potential as
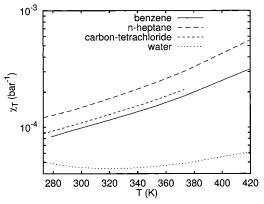
$$\mu^{ex} \approx T\rho^2(T)x(v) + Ty(v) \qquad (34)$$

where the functions $x(v) = k_B v^2/2\sigma^2$ and $y(v) = k_B \ln(2\pi\sigma^2)/2$ depend only on the solute volume, not on the temperature. The contributions of the various terms to the entropy convergence are illustrated schematically in Figure 11. The term $Ty(v)$ in eq 33 is generally small. If we neglect $Ty(v)$, the solvation entropies eq 31 converge exactly at zero entropy for solutes of different size, and the temperature of convergence corresponds to the maximum of $T\rho^2(T)$ along the saturation curve. When the second term $Ty(v)$ is included, the entropy at convergence is different from zero, but the convergence is still exact. However, both $x(v)$ and $y(v)$ show weak temperature dependences. When those are considered as well, the resulting entropy convergence is no longer exact but occurs over a temperature range that is several 10 K wide for the solutes considered here.

Our analysis shows that the main factors leading to an entropy convergence are derived from the properties of pure water. They are (1) the nonmonotonic behavior of $T\rho^2(T)$ along the saturation curve and (2) the weak temperature dependence of the particle-number fluctuations $\sigma^2(T, v)$ for solute excluded volumes. The macroscopic analog of σ^2 is the isothermal compressibility χ_T. For macroscopic volumes v, eq 23 relates the two, $\sigma^2 = \rho^2 v k_B T \chi_T$. Figure 12 compares the isothermal

Figure 11. Schematic representation of the different factors resulting in approximate convergence of solvation entropies.
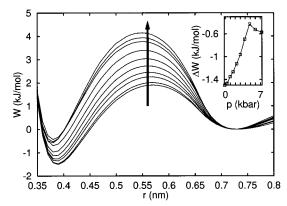

Figure 12. Comparison of the isothermal compressibility of water and nonpolar solvents as a function of temperature along their respective saturation curves. Data are taken from ref 90.

compressibility of water and several organic solvents up to their critical point as a function of temperature. Indeed, we find that water shows far weaker temperature variations of χ_T than the organic solvents, which can be seen as the origin of the entropy convergence. In the macroscopic limit, the variance $\sigma^2 = \rho^2 v k_B T \chi_T$ is a product of $T \rho^2(T)$ with a maximum at about 440 K and χ_T with a minimum at about 320 K. This results in only small variations of σ^2 in the range of temperatures between 273 and 420 K.

V. Pressure Denaturation of Proteins

a. Denaturation by Water Transfer into the Protein Interior. Proteins can be denatured by pressures of typically

Figure 13. Pressure dependence of the PMF between two methane-like solutes in water. The PMF's were calculated from information theory using a flat default model.[15] A methane−methane Lennard-Jones interaction was added. SPC water[57] $g(r)$'s were used. The arrows indicate changes with increasing pressures from −160 to 7250 bar.

a few kilobar.[19−26] This pressure-induced unfolding has been a long-standing puzzle in our understanding of protein stability. The "liquid-hydrocarbon model" of protein stability[11] explains unfolding as a transfer of predominantly hydrophobic residues from the protein interior into the aqueous solvent. Indeed, this model accurately describes the thermodynamics of temperature denaturation, in particular, the convergence of the entropies of unfolding. However, as Kauzmann[13] pointed out, such a description fails to explain the pressure denaturation of proteins. In particular, the volume changes associated with transferring hydrocarbons from a nonpolar phase into water exhibit behavior exactly opposite to that upon pressure unfolding as a function of pressure. The volume change of hydrocarbon transfer is negative at low pressure and positive at high pressure;[91] the volume change of protein unfolding is positive at low pressure and negative at high pressure.[13]

To explain the pressure denaturation of proteins, we invoke additional information about the structural properties of pressure-denatured proteins. Nuclear magnetic resonance (NMR) measurements reveal considerably more structural organization in pressure-denatured proteins compared to that in temperature-denatured proteins.[27] These and other experiments[21−24] indicate that the pressure-denatured proteins are relatively more compact than temperature-denatured proteins. Accordingly, we depart from the commonly used model explaining protein unfolding thermodynamics as a transfer of nonpolar residues from the protein interior into solution. Instead, we describe pressure denaturation as a transfer of water molecules from the aqueous phase into the hydrophobic core of a protein.

To quantify this inverted "liquid-hydrocarbon model," we focus on the stability of hydrophobic aggregates formed in water as a function of pressure. Aggregate formation of spherical, methane-size solutes serves as an idealized model of the stability of protein hydrophobic cores. The free energy of forming such aggregates can be expressed in terms of two-body and higher order PMFs between the methane-size solutes in water. In the following, we will study the pair and three-body interactions of methane-like solutes in water which control the stability and formation of larger aggregates.

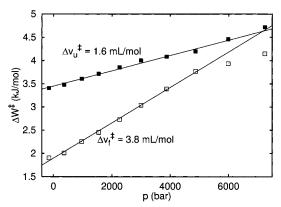**b. Effect of Pressure on Hydrophobic Interactions.** Figure 13 shows the PMFs $W(r)$ between two methane-like particles in water for pressures up to about 7 kbar (700 MPa) calculated using IT.[15] The PMF's exhibit two minima, a contact minimum at about 0.4 nm distance and a solvent-separated minimum at a distance of about 0.7 nm. The two minima are separated by the desolvation barrier. The PMF's are normalized at the

Feature Article

J. Phys. Chem. B, Vol. 102, No. 51, 1998 **10479**

solvent-separated minimum to illustrate that the contact minimum loses importance with increasing pressure. The free energy of the contact minimum increases relative to the solvent-separated minimum by about 0.9 kJ/mol when the pressure is increased from 1 bar to 7 kbar. In addition, the desolvation barrier between the two minima also increases with increasing pressure. Similar pressure destabilization of contact configurations was observed for three methane molecules in contact.[15]

The effect of pressure on pair PMF's between two methane molecules has also been studied by computer simulation.[92] These simulation calculations showed a pressure destabilization of contact pairs that is comparable in magnitude to the IT calculations. In addition, simulation calculations also showed the formation of methane aggregates in water at low pressures that dissolved at high pressures.[93]

The pressure destabilization of hydrophobic contact configurations can be understood from the following simplified model: At low pressures, the interstitial space between two large nonpolar solutes is energetically unfavorable for water molecules.[55,94] As the pressure increases, the space between the nonpolar solutes is more likely to be occupied by water, increasing the importance of solvent-separated configurations relative to contact configurations. A more detailed analysis indeed shows that the destabilizing effect of pressure on hydrophobic contacts increases with increasing size of the two nonpolar solutes.[15]

c. Stability of Proteins. We have shown that the stability of hydrophobic aggregates decreases with increasing pressure as a result of water penetration. When applied to the hydrophobic-core model of proteins, we predict that pressure denatures proteins by swelling.[15] A swelling mechanism has also been proposed for urea-induced protein denaturation.[95] Under sufficiently high pressures, water molecules will intercalate into the hydrophobic protein interior. The resulting structures of pressure-denatured proteins are predicted to be more ordered and more compact than those of temperature-denatured proteins. Recent small-angle scattering experiments[28] indeed showed that the pressure-denatured staphylococcal nuclease protein has a considerably smaller radius of gyration of $R_g \approx 3.5$ nm compared to the temperature-denatured protein with $R_g \approx 4.6$ nm.

d. Formation of Clathrate Hydrates. This physical picture of pressure denaturation of proteins is relevant also for the formation of clathrate hydrates, crystalline compounds forming at elevated pressures from nonpolar molecules and water. As solid deposits in gas pipelines, clathrate hydrates cause problems in natural gas transmission. Methane—water clathrate hydrates, for instance, form at pressures above about 44 MPa at a temperature of 298 K, with a stoichiometry of about 6 to 7 water molecules per methane and a methane—methane nearest-neighbor distance of about 0.62—0.74 nm.[96] At lower pressures, the two fluid phases separate. Formation of the clathrate structure is consistent with stabilizing the solvent-separated minimum in the methane—methane PMF relative to the contact minimum, as predicted from the analysis of pressure effects on hydrophobic interactions. In addition, the present theory predicts that larger hydrocarbons require lower pressure for clathrate formation,[15] in agreement with the experimental observations that led to the gas-gravity method of phase determination.[96]

e. Pressure Effects on Protein Folding Kinetics. We noted before that increasing pressure results in a higher desolvation barrier between the contact configuration and the solvent-separated minimum. Figure 14 shows the barrier heights $\Delta W_f^{\ddagger}$

Figure 14. Pressure dependence of the desolvation barrier between the contact and solvent-separated minimum in the methane—methane PMF of Figure 13. The activation free energy for forming (open squares) and breaking hydrophobic contacts (filled squares) is shown as a function of pressure.
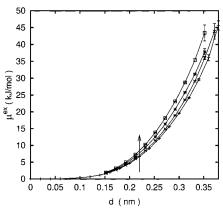
and $\Delta W_u^{\ddagger}$ from the solvent-separated and contact minimum, respectively, as a function of pressure. Thus, $\Delta W_f^{\ddagger}$ and $\Delta W_u^{\ddagger}$ are the barriers for forming and breaking hydrophobic contact configurations, corresponding to "folding" and "unfolding" reactions, respectively. We find that $\Delta W_f^{\ddagger}$ and $\Delta W_u^{\ddagger}$ both increase approximately linearly with increasing pressure. Activation volumes defined as $\Delta v_{f/u}^{\ddagger} = \partial \Delta W_{f/u}^{\ddagger}/\partial p$ are both positive, $\Delta v_f^{\ddagger} = 3.8$ mL/mol and $\Delta v_u^{\ddagger} = 1.6$ mL/mol, for folding and unfolding reactions, respectively. Increasing pressure is thus expected to slow down both the "folding" and the "unfolding" reactions.

Indeed, experimental studies of the pressure-dependent folding and unfolding kinetics of the protein staphylococcal nuclease showed a reduction of both rates with increasing pressure.[97] The experimentally observed activation volumes for folding and unfolding of staphylococcal nuclease are $\Delta V_f^{\ddagger} = 92$ mL/mol and $\Delta V_u^{\ddagger} = 20$ mL/mol, respectively. From the ratio of overall experimental activation volumes and theoretical activation volumes calculated per hydrophobic contact, we can estimate the number of hydrophobic contacts broken in the folding transition state. For staphylococcal nuclease we estimate that number to be between 10 and 25, in good agreement with the predictions of energy landscape theory.[15,98]

VI. Salt Effects on Hydrophobic Hydration

Addition of salts to water generally reduces the solubility of nonpolar solutes. The Hofmeister series[29] ranks salts, in part, according to this reduction of the solubility of nonpolar compounds. Here, we do not attempt to provide a complete description of salt effects on hydrophobic hydration. Instead, we present some preliminary results for the solubility of small hard-sphere solutes in a solution of sodium chloride (NaCl) in water. In particular, we compare results for NaCl concentrations of 1, 3, and 5 mol/L as well as pure water. The three salt solutions were studied using molecular dynamics simulations extending over 1 ns each. For simulation details, see ref 99.

Figure 15 shows the excess chemical potential of spherical solutes as a function of their exclusion radius d with water. The solute—solvent interactions are modeled as those of hard spheres with radii $R_w = 0.132$ nm of water, $R_{Na} = 0.085$ nm of Na^+, and $R_{Cl} = 0.18$ nm of Cl^-. The exclusion radii with water, Na^+, and Cl^- are $d = R + R_w$, $R + R_{Na}$, and $R + R_{Cl}$, respectively, where R is the solute hard-sphere radius. We find that adding salt indeed increases μ^{ex} and thus decreases the solubility for a solute of a given size. For a methane-size solute

Figure 15. Excess chemical potential of hard-sphere solutes in aqueous NaCl solution as a function of solute size, given by the exclusion radius with water, and salt concentration (squares, 5 mol/L; stars, 3 mol/L; crosses, 1 mol/l: plus, pure water).

($d = 0.33$ nm), the excess chemical potential increases by about 10 kJ/mol from about 34 to 44 kJ/mol when increasing the NaCl concentration from 0 to 5 mol/L.

To describe the salt dependence using the IT approach, we extend our formulation to solvent mixtures. For ionic solutes, the strong interactions between water and ions give rise to the formation of compact hydrated ions resulting in nontrivial density fluctuations near ions. Therefore, instead of trying to model the full distribution of particle number fluctuations $p(n_W, n_{Na}, n_{Cl})$, we focus on a more tractable subset, which contains the probability of the event we are ultimately interested in, $p(n_W = 0, n_{Na} = 0, n_{Cl} = 0)$. Further, we factorize this probability into an ionic part and a conditional water part

$$p(n_W = 0, n_{Na} = 0, n_{Cl} = 0) =$$
$$p(n_{Na} = 0, n_{Cl} = 0) \, p(n_W = 0 | n_{Na} = 0, n_{Cl} = 0) \quad (35)$$

where $p(n_W = 0 | n_{Na} = 0, n_{Cl} = 0)$ is the conditional probability of having no water-oxygen atoms in the water exclusion volume, given that there are no ions in the respective ion exclusion volumes. Such a factorization combined with accurate simulation data provides insights into salt effects on hydrophobic solubilities at a molecular level. The contributions to the solute chemical potential, $-k_B T \ln p(n_{Na} = 0, n_{Cl} = 0)$ and $-k_B T \ln p(n_W = 0 | n_{Na} = 0, n_{Cl} = 0)$ both increase with increasing NaCl concentration. The increase in the salt contribution is primarily due to an increase in the mean of the $p(n_{Na}, n_{Cl})$ distribution. Interestingly, the mean of $p(n_W | n_{Na} = 0, n_{Cl} = 0)$ is approximately independent of salt concentration. It is the decrease in the variance of this conditional water distribution with increasing NaCl concentration that leads to a decrease in $p(n_W = 0 | n_{Na} = 0, n_{Cl} = 0)$. The direct salt effect of the reduction in free volume due to overlap with salt ions and the indirect salt effect of changing the water structure account for roughly one-half each of the total increase in solute chemical potentials.

VII. New Directions: Cavity Expulsion and Area Laws

We mentioned in section II.e that for macroscopic solutes physical effects intrude that are not captured in the simplest IT models. This is a consequence of the multiphasic nature of water. In the limit of large solutes, the solvation chemical potential is largely determined by the free energy of forming a vapor bubble of appropriate size. The free energy of forming large bubbles can be approximated by the product of surface

area and liquid−vapor surface tension, since the contribution from the pressure−volume work is small for water.[38] Accordingly, we expect that the solvation chemical potential grows with the surface area for large solutes. Stillinger[38] gave a justification of this based on the water structure near a large hard solute. The contact-value theorem gives, in the limit of a flat hard wall, a water density at contact of about 7.4×10^{-4} times the bulk density of water. Stillinger argued that this "dewetting" implies the presence of a molecularly thick vapor layer near a hard wall, and as a result, area laws with surface tension coefficients similar to that of the liquid−vapor surface tension of water.

In an attempt to bridge the gap between microscopic and macroscopic solvation behavior, we have recently developed a quantitative description of the solvation of nonpolar solutes as a function of their size.[55] The water structure near spherical[55] and nonspherical Lennard-Jones solutes[100,101] was found to be largely insensitive to the details of the solute−water interactions except for the solute size, motivating the use of perturbation theory. For spherical solutes, we find that the radial distributionfunction of water around the solute can be described accurately by

$$g_{sw}(r) = \exp[-\beta u_{rep}(r) - \beta \omega(r) + C(r)] \quad (36)$$

where $u_{rep}(r)$ is the repulsive solute-water interaction from, e.g., Weeks−Chandler−Anderson separation;[102] $C(r)$ is a renormalized attractive interaction; and $\omega(r)$ represents the free energy of a test water molecule that does not interact with the solute as a function of the distance r from the solute,[55] thus containing the nontrivial solvent contributions. Interestingly, $\omega(r)$ is directly related to the one-body Lagrange multiplier $\omega^{(1)}(\mathbf{r})$ of the continuous IT eq 11. We find that $\omega(r)$ is dominated by a contribution $\omega_0(r - r_0)$ that is identical for various solutes except for a simple radial translation with the solute size r_0. The remainder $\Delta\omega(r - r_0)$, however, changes nontrivially with the solute size, acting as a cavity-expulsion potential for the test water molecule.

The cavity-expulsion potential $\Delta\omega(r - r_0)$ quantifies primarily the loss of energetic interactions of a test water molecule as it crosses the solute−water interface from the water phase towards the center of the solute. For small solutes, $\Delta\omega(r - r_0)$ is negligible. As the solute size increases, this loss of interactions becomes important, reaching $-\mu_w^{ex}$, the negative excess chemical potential of water, in the limit of large solutes. For solutes of diameters more than about 0.5 nm the cavity expulsion results in a slight depression in the water density at the solute-water interface. We find that this "weak dewetting" with increasing solute size is sufficient to give an approximate surface-area dependence of the solvation chemical potential, which would otherwise be dominated by solute volume terms.[55]

VIII. Concluding Remarks

How is water different from hydrocarbon liquids as a solvent for nonpolar solutes? This is the foremost question asked of theories of hydrophobic effects and several of the points above constitute relevant parts of the answer. It is appropriate therefore to ask this question more specifically and to organize features of the answer that are provided by the IT models considered here. One basic aspect of the answer is straightforward and on that score we do not contribute anything further: water is different because of the mechanical potential energies of the

Feature Article

J. Phys. Chem. B, Vol. 102, No. 51, 1998 **10481**

interactions among water molecules, including hydrogen bonding, orientational specificity, and cooperativity.

In the context of solvation thermodynamics, the question how water differs from other solvents solicits information about a particular structural pattern of the solvent that might be principally responsible for hydrophobic hydration free energies. For example, clathrate-like structures have been invoked to explain hydrophobic hydration phenomena.[103] The answer given by the IT model is that water differs from common hydrocarbon solvents, in the first place, because the distribution of pairs of exclusion spheres, oxygen−oxygen sites in water, is distinctive and has a distinctive temperature dependence. In the second place, the isothermal compressibility of water, which can be obtained by integration of the oxygen-oxygen distribution, is insensitive to temperature compared to the same property of organic solvents. Since the minimum in the temperature dependence of the isothermal compressibility is very distinctive, this answer is remarkable and remarkably simple.

From our analysis of pressure effects on hydrophobic interactions and protein stability, we can deduce further peculiarities of water. Increasing the pressure in water shifts the balance from attractive and directional hydrogen-bonding forces to repulsive and isotropic packing forces between water molecules.[104] This results in "energetic frustration" of water molecules in the water phase,[105] which in turn reduces the relative cost of incorporating water molecules into a hydrophobic aggregate. At least two factors make water special in this context: its large negative excess chemical potential prevents water from penetrating hydrophobic aggregates under normal conditions,[55] thus driving the formation of protein hydrophobic cores. Under sufficiently high pressure, however, the relatively small water molecules occupy previously empty cavities, exploiting imperfections in the packing of the protein interior. Note that the small size of water molecules here is not used as an argument that "interstitial" cavities are smaller in water than in typical organic liquids,[76,77] as discussed in section II.f, but that water molecules can occupy small cavities in the protein interior. This incorporation of water molecules is favored further by the versatility of water molecules which can form favorable hydrogen-bonding interactions in many different environments, particularly in the interior of a protein which is never entirely nonpolar.

These arguments also explain in part the success of simple theories, such as SPT and PC, that take no special account of the known details of hydrophobic solvation patterning. These theories yield satisfactory predictions for the simplest hydrophobic effects in part because they incorporate information about the equation of state and the oxygen-atom pair correlations of water. A next stage of basic molecular theory of hydrophobic effects will surely address the hydration structure in more detail while at the same time preserving equation of state information such as the low, temperature insensitive values of the isothermal compressibility that have been identified as particularly important.

IT models of the solvation thermodynamics can easily be generalized to various aqueous and nonaqueous solvents and mixtures, combined with other approaches, or extended to "unusual" models of water, such as a recently proposed two-dimensional model of water[106] or an isotropic water model without directional hydrogen-bond interactions.[83] We have successfully adapted the method to study the solubility of small molecules in polymeric fluids.[107,108] Crooks and Chandler[109] compared solvation chemical potentials of hard spheres of varying sizes in hard-sphere fluids to simulation data, finding

that a Gibbs prior gives a good description of the density fluctuations and the solvation thermodynamics. Applications of the IT method to study phase equilibria have been suggested.[110] Lum, Chandler, and Weeks[111] have combined field-theoretical methods[52] with the IT approach to describe the solvation thermodynamics and structure of mesoscopic and macroscopic spherical solutes in water which is tightly associated with "dewetting" of the solute surface.[38,55]

The development of IT models is an ongoing effort targeting several directions. A better description for molecularly large solutes can be expected from improved, physically motivated default models that incorporate the multiphasic nature of water to account for the free energy of forming microscopic vapor bubbles.[111] IT models can easily be generalized to study hydrophobic interactions in inhomogeneous environments, for instance, to describe ligand binding to proteins. Section IIc gives an outline of a continuous IT, which establishes connections to the concepts of cavity expulsion and dewetting of nonpolar surfaces.[55] The volume stratification discussed in section II.d leads naturally to predictions of the hydration structure.

In conclusion, we believe that the basic IT model provides a simple theoretical framework to study many hydrophobic phenomena on a molecular scale, as it already led to a new understanding of the temperature dependence of hydrophobic hydration,[14] and resulted in a new description of the pressure denaturation of proteins.[15]

References and Notes

(1) Kauzmann, W. *Adv. Protein Chem.* **1959**, *14*, 1.
(2) Tanford, C. *The Hydrophobic Effect: Formation of Micelles and Biological Membranes*; John Wiley & Sons: New York, 1973.
(3) Dill, K. A. *Biochemistry* **1990**, *29*, 7133.
(4) Blokzijl, W.; Engberts, J. B. F. N. *Angew. Chem., Int. Ed. Engl.* **1993**, *32*, 1545.
(5) Fink, A. L. *Folding Design* **1998**, *3*, R9.
(6) Privalov, P. L. *Adv. Protein Chem.* **1979**, *33*, 167.
(7) Privalov, P. L.; Gill, S. J. *Adv. Protein Chem.* **1988**, *39*, 191.
(8) Makhatadze, G. I.; Privalov, P. L. *Adv. Protein Chem.* **1995**, *47*, 307.
(9) Richards, F. M. *J. Mol. Biol.* **1974**, *82*, 1.
(10) Buckle, A. M.; Henrick, K.; Fersht, A. R. *J. Mol. Biol.* **1993**, *234*, 847.
(11) Baldwin, R. L. *Proc. Natl. Acad. Sci. U.S.A.* **1986**, *83*, 8069.
(12) Baldwin, R. L.; Muller, N. *Proc. Natl. Acad. Sci. U.S.A.* **1992**, *89*, 7110.
(13) Kauzmann, W. *Nature (London)* **1987**, *325*, 763.
(14) Garde, S.; Hummer, G.; García, A. E.; Paulaitis, M. E.; Pratt, L. R. *Phys. Rev. Lett.* **1996**, *77*, 4966.
(15) Hummer, G.; Garde, S.; García, A. E.; Paulaitis, M. E.; Pratt, L. R. *Proc. Natl. Acad. Sci. U.S.A.* **1998**, *95*, 1552.
(16) Privalov, P. L.; Khechinashvili, N. N. *J. Mol. Biol.* **1974**, *86*, 665.
(17) Makhatadze, G. I.; Privalov, P. L. *Adv. Protein Chem.* **1995**, *47*, 307.
(18) Privalov, P. L.; Makhatadze, G. I. *J. Mol. Biol.* **1993**, *232*, 660.
(19) Brandts, J. F.; Oliveira, R. J.; Westort, C. *Biochemistry* **1970**, *9*, 1038.
(20) Zipp, A.; Kauzmann, W. *Biochemistry* **1973**, *12*, 4217.
(21) Heremans, K. *Annu. Rev. Biophys. Bioeng.* **1982**, *11*, 1.
(22) Weber, G.; Drickamer, H. G. *Quart. Rev. Biophys.* **1983**, *16*, 89.
(23) Silva, J. L.; Weber, G. *Annu. Rev. Phys. Chem.* **1993**, *44*, 89.
(24) Jonas, J.; Jonas, A. *Annu. Rev. Biophys. Biomol. Struct.* **1994**, *23*, 287.
(25) Royer, C. A. *Methods Enzymol.* **1995**, *259*, 357.

(26) Silva, J. L.; Foguel, D.; Da Poian, A. T.; Prevelige, P. E. *Curr. Opin. Struct. Biol.* **1996**, *6*, 166.

(27) Zhang, J.; Peng, X.; Jonas, A.; Jonas, J. *Biochemistry* **1995**, *34*, 8631.

(28) Panick, G.; Malessa, R.; Winter, R.; Rapp, G.; Frye, K. J.; Royer, C. A. *J. Mol. Biol.* **1998**, *275*, 389.

(29) Baldwin, R. L. *Biophys. J.* **1996**, *71*, 2056.

(30) Frank, H. S.; Evans, M. W. *J. Chem. Phys.* **1945**, *13*, 507.

(31) Némethy, G.; Scheraga, H. A. *J. Chem. Phys.* **1962**, *36*, 3382.

(32) Ben-Naim, A. *Hydrophobic Interactions*; Plenum: New York, 1980.

(33) Besseling, N. A. M.; Lyklema, J. *J. Phys. Chem. B* **1997**, *101*, 7604.

(34) Madan, B.; Sharp, K. *J. Phys. Chem. B* **1997**, *101*, 11237.

(35) Note that it is not within the scope of this article to review the entire literature devoted to the hydrophobic effect. An electronic literature search produced over 28 000 publications that contain the word hydrophobic in the title or list of keywords since 1974!

(36) Reiss, H.; Frisch, H. L.; Lebowitz, J. L. *J. Chem. Phys.* **1959**, *31*, 369.

(37) Pierotti, R. A. *J. Phys. Chem.* **1963**, *67*, 1840.

(38) Stillinger, F. H. *J. Solut. Chem.* **1973**, *2*, 141.

(39) Hermann, R. B. *J. Phys. Chem.* **1972**, *76*, 2754.

(40) Chothia, C. *Nature* **1974**, *248*, 338.

(41) Oobatake, M.; Ooi, T. *Prog. Biophys. Mol. Biol.* **1993**, *59*, 237.

(42) Sharp, K. A.; Nicholls, A.; Fine, R. F.; Honig, B. *Science* **1991**, *252*, 106.

(43) Simonson, T.; Brunger, A. T. *J. Phys. Chem.* **1994**, *98*, 4683.

(44) Giesen, D. J.; Cramer, C. J.; Truhlar, D. G. *J. Phys. Chem.* **1994**, *98*, 4141.

(45) Tunon, I.; Silla, E.; Pascualahuir, J. L. *J. Phys. Chem.* **1994**, *98*, 377.

(46) Fukunishi, Y.; Suzuki, M. *J. Phys. Chem.* **1996**, *100*, 5634.

(47) Pratt, L. R.; Chandler, D. *J. Chem. Phys.* **1977**, *67*, 3683.

(48) Lazaridis, T.; Paulaitis, M. E. *J. Phys. Chem.* **1992**, *96*, 3847.

(49) Pangali, C.; Rao, M.; Berne, B. J. *J. Chem. Phys.* **1979**, *71*, 2975.

(50) Hummer, G.; Garde, S.; García, A. E.; Pohorille, A.; Pratt, L. R. *Proc. Natl. Acad. Sci. U.S.A.* **1996**, *93*, 8951.

(51) Jaynes, E. T. In *E. T. Jaynes: Papers on Probability, Statistics, and Statistical Physics*; Rosenkrantz, R. D., Ed.; Reidel: Dordrecht, Holland, 1983.

(52) Chandler, D. *Phys. Rev. E* **1993**, *48*, 2898.

(53) Berne, B. J. *Proc. Natl. Acad. Sci. U.S.A.* **1996**, *93*, 8800.

(54) Percus, J. K. *J. Phys. IV* **1993**, *3*, 49.

(55) Hummer, G.; Garde, S. *Phys. Rev. Lett.* **1998**, *80*, 4193.

(56) Pollack, G. L. *Science* **1991**, *251*, 1323.

(57) Berendsen, H. J. C.; Postma, J. P. M.; van Gunsteren, W. F.; Hermans, J. In *Intermolecular Forces*; Pullman, B., Ed.; Reidel: Dordrecht, Holland, 1981; pp 331−342.

(58) Hummer, G.; Soumpasis, D. M. *Phys. Rev. E* **1994**, *49*, 591.

(59) Shore, J. E.; Johnson, R. W. *IEEE Trans. Inf. Theory* **1980**, *26*, 26.

(60) Berendsen, H. J. C.; Grigera, J. R.; Straatsma, T. P. *J. Phys. Chem.* **1987**, *91*, 6269.

(61) Pratt, L. R.; Garde, S.; Hummer, G. *Proceedings of the NATO Advanced Study Institute: New Approaches to old and new Problems in Liquid State Theory,* Patti Marina (Messina) Italy, July 1998; submitted [LA-UR 98-98-2712].

(62) Widom, B. *J. Chem. Phys.* **1963**, *39*, 2808.

(63) Stratonovich, R. L. *J. Exp. Theoret. Phys. USSR* **1955**, *28*, 409 (English translation in *Soviet Physics−JETP* **1955**, *1*, 254).

(64) Hill, T. L. *J. Chem. Phys.* **1958**, *28*, 1179.

(65) Guinier, A. *Ann. Phys. (Paris)* **1939**, *1*, 11.

(66) Mayer, J. E.; Montroll, E. *J. Chem. Phys.* **1941**, *8*, 2.

(67) Riordan, J. *An Introduction to Combinatorial Analysis*; Princeton University Press: Princeton, NJ, 1978; p 32.

(68) Reiss, H. *Adv. Chem. Phys.* **1965**, *9*, 1.

(69) Pratt, L. R.; Pohorille, A. *Proc. Natl. Acad. Sci. U.S.A.* **1992**, *89*, 2995.

(70) Pohorille, A.; Pratt, L. R. *J. Am. Chem. Soc.* **1990**, *112*, 5066.

(71) Pratt, L. R.; Pohorille, A. In *Proceedings of the EBSA (Association of the European Biophysical Societies) 1992 International Workshop on Water-Biomolecule Interactions*; Palma, M. U., Palma-Vittorelli, M. B., Parak, F., Eds.; Societá Italiana de Fisica: Bologna, 1993; pp 261−268.

(72) Guillot, B.; Guissani, Y. *J. Chem. Phys.* **1993**, *99*, 8075.

(73) Forsman, J.; Jönsson, B. *J. Chem. Phys.* **1994**, *101*, 5116.

(74) Beutler, T. C.; Béguelin, D. R.; van Gunsteren, W. F. *J. Chem. Phys.* **1995**, *102*, 3787.

(75) Stamatopoulou, A.; Ben-Amotz, D. *J. Chem. Phys.* **1998**, *108*, 7294.

(76) Lee, B. *Biopolymers* **1985**, *24*, 813.

(77) Lee, B. *Biopolymers* **1991**, *31*, 993.

(78) Richards, F. M. *Sci. Am.* **1991**, *264*, 54.

(79) Haymet, A. D. J.; Silverstein, K. A. T.; Dill, K. A. *Faraday Discuss.* **1996**, *103*, 117.

(80) Watanabe, K.; Andersen, H. C. *J. Phys. Chem.* **1986**, *90*, 795.

(81) Smith, D. E.; Haymet, A. D. J. *J. Chem. Phys.* **1993**, *98*, 6445.

(82) van Belle, D.; Wodak, S. J. *J. Am. Chem. Soc.* **1993**, *115*, 647.

(83) Head-Gordon, T. *J. Am. Chem. Soc.* **1995**, *117*, 501.

(84) Garde, S.; Hummer, G.; Paulaitis, M. E. *Faraday Discuss.* **1996**, *103*, 125.

(85) Lüdemann, S.; Abseher, R.; Schreiber, H.; Steinhauser, O. *J. Am. Chem. Soc.* **1997**, *119*, 4206.

(86) Hummer, G.; Pratt, L. R.; García, A. E. *J. Phys. Chem.* **1996**, *100*, 1206.

(87) Jorgensen, W. L.; Madura, J. D.; Swenson, C. J. *J. Am. Chem. Soc.* **1984**, *106*, 6638.

(88) Beglov, D.; Roux, B. *J. Chem. Phys.* **1994**, *100*, 9050.

(89) Dill, K. A. *Science* **1990**, *250*, 297.

(90) Rowlinson, J. S.; Swinton, F. L. *Liquids and Liquid Mixtures*; Butterworths: London, 1982.

(91) Sawamura, S.; Kitamura, K.; Taniguchi, Y. *J. Phys. Chem.* **1989**, *93*, 4931.

(92) Payne, V. A.; Matubayasi, N.; Murphy, L. R.; Levy, R. M. *J. Phys. Chem. B* **1997**, *101*, 2054.

(93) Wallqvist, A. *J. Chem. Phys.* **1992**, *96*, 1657.

(94) Wallqvist, A.; Berne, B. J. *J. Phys. Chem.* **1995**, *99*, 2893.

(95) Wallqvist, A.; Covell, D. G.; Thirumalai, D. *J. Am. Chem. Soc.* **1998**, *120*, 427.

(96) Sloan, E. D., Jr. *Clathrate Hydrates of Natural Gases*; M. Dekker: New York, 1990.

(97) Vidugiris, G. J. A.; Markley, J. L.; Royer, C. A. *Biochemistry* **1995**, *34*, 4909.

(98) Bryngelson, J. D.; Onuchic, J. N.; Socci, N. D.; Wolynes, P. G. *Proteins Struct. Funct. Genet.* **1995**, *21*, 167.

(99) Hummer, G.; Soumpasis, D. M.; Neumann, M. *J. Phys.: Condens. Matt.* **1994**, *6*, A141.

(100) Garde, S.; Hummer, G.; García, A. E.; Pratt, L. R.; Paulaitis, M. E. *Phys. Rev. E* **1996**, *53*, R4310.

(101) Ashbaugh, H. S.; Paulaitis, M. E. *J. Phys. Chem.* **1996**, *100*, 1900.

(102) Weeks, J. D.; Chandler, D.; Andersen, H. C. *J. Chem. Phys.* **1971**, *54*, 5237.

(103) Head-Gordon, T. *Proc. Natl. Acad. Sci. U.S.A.* **1995**, *92*, 8308.

(104) Stillinger, F. H.; Rahman, A. *J. Chem. Phys.* **1974**, *61*, 4973.

(105) Sciortino, F.; Geiger, A.; Stanley, H. E. *Nature (London)* **1991**, *354*, 218.

(106) Silverstein, K. A. T.; Haymet, A. D. J.; Dill, K. A. *J. Am. Chem. Soc.* **1998**, *120*, 3166.

(107) Garde, S.; Khare, R.; Hummer, G. Unpublished manuscript.

(108) Cuthbert, T. R.; Wagner, N. J.; Paulaitis, M. E. *Macromolecules* **1997**, *30*, 3058.

(109) Crooks, G. E.; Chandler, D. *Phys. Rev. E* **1997**, *56*, 4217.

(110) Wu, J. Z.; Prausnitz, J. M. *Ind. Eng. Chem. Res.* **1998**, *37*, 1634.

(111) Lum, K.; Chandler, D.; Weeks, J. D. **1998**. Submitted for publication.